Hindawi
International Journal of Aerospace Engineering
Volume 2023, Article ID 9526861, 13 pages
https://doi.org/10.1155/2023/9526861

Research Article

Sensitivity and Consistency Analysis of BDS-3 GEO Satellite Orbit Maneuver Detection

Yage Miao,[1,2] Rui Tu,[1,2,3] Ju Hong,[1,2] Shixuan Zhang,[1,2] Fangxin Li,[1,2] Mingyue Liu,[1,2] and Xiaochun Lu[1,2,3]

[1]*National Time Service Center, Chinese Academy of Sciences, Shu Yuan Road, 710600 Xi'an, China*
[2]*University of Chinese Academy of Sciences, Yu Quan Road, 100049 Beijing, China*
[3]*Key Laboratory of Precision Navigation and Timing Technology, Chinese Academy of Sciences, Shu Yuan Road, 710600 Xi'an, China*

Correspondence should be addressed to Rui Tu; turui-2004@126.com

Received 2 January 2023; Revised 27 February 2023; Accepted 28 February 2023; Published 31 March 2023

Academic Editor: Jinchao Chen

In this study, 22 maneuvering events of C59 and C60 geostationary equatorial orbit (GEO) satellites of the BeiDou global navigation satellite system (BDS-3) in 2021 were detected and analyzed based on a time-differenced carrier phase velocity measurement algorithm combined with a broadcast ephemeris and station data. We set different empirical thresholds to analyze the effect of threshold selection on the maneuvering detection sensitivity. The sensitivity and consistency of this algorithm for GEO satellite maneuvering detection were analyzed by combining BDS-3 with other Global navigation satellite systems (GNSS) and selecting different geographic stations. The results demonstrate that changing the threshold significantly affects the maneuvering detection of C60, with the optimal maneuvering thresholds of C59 and C60 being 0.045 and 0.02, respectively. A combination of BDS-3 and GPS with equal weights was identified to be most suitable for maneuvering detection of GEO satellites. For any specific maneuver, the difference between the maneuvering time detection of C59 by stations at different geographical locations was no more than 1 min. During the maneuvering detection of C60, the start time of maneuvering detected by African stations was 4.26–8.61 min earlier than that detected by the Chinese and Australian stations, and the end time of maneuvering detected by the African stations was consistent with that detected by the Chinese and Australian stations.

1. Introduction

Since the establishment of the Beidou-3 global navigation satellite system (BDS-3) on July 31, 2020, positioning, navigation, and timing (PNT) services have been provided in many fields worldwide [1]. BDS-3 uses a hybrid constellation comprising 24 medium earth orbit (MEO) satellites, three geostationary orbit (GEO) satellites, and three inclined geosynchronous orbit (IGSO) satellites [2, 3]. To maintain geosynchronous characteristics, GEO satellites perform orbital maneuvers approximately once a month, and IGSO satellites perform orbital maneuvers approximately once every 6 months [4]. During orbital maneuvers, the actual position of satellites differs by tens of kilometers from the predicted orbital position [5]. However, for practical applications, only the health status of the satellite is publicly marked in the hourly broadcast ephemeris; therefore, satellite maneuvering information cannot be obtained. Consequently, a large quantity of valid data is lost, leading to a significant difference in the service performance of satellites before and after maneuvering. Therefore, accurate and timely detection of the orbital maneuvering periods of satellites is essential.

In recent years, several scholars have investigated orbital maneuver detection. Du et al. determined the orbital maneuvres of the GEO satellites using China area positioning system data; however, it is not suitable for the BDS [6]. Tu et al. proposed a monitoring model combining the principle of time-differenced velocity estimation and multistation observations of BDS, which allowed the estimation of three-dimensional dynamic changes in orbital maneuvers

```
C59 2021 02 09 12 00 00-9.398208931088E-07-7.194245199571E-14 0.000000000000E+00
     1.000000000000E+00 5.535625000000E+02 6.591345984589E-09-2.983460605544E+00
     1.832097768784E-05 2.048010937870E-04 1.246342435479E-05 6.493560083389E+03
     2.160000000000E+05-1.988373696804E-07 2.966231261953E-01 1.136213541031E-07
     8.619359424060E-02-3.790468750000E+02 2.031727138025E+00-5.640592096159E-09
     7.993190091308E-10 0.000000000000E+00 7.880000000000E+02 0.000000000000E+00
     2.000000000000E+00 0.000000000000E+00 4.220000000000E-08 4.220000000000E-08
     2.160276000000E+05 1.000000000000E+00
C59 2021 02 09 13 00 00-9.405193850398E-07-1.234568003383E-13 0.000000000000E+00
     2.000000000000E+00 6.790312500000E+02 7.799610599374E-09-2.723779649910E+00
     2.240063622594E-05 2.056830562651E-04 2.178363502026E-06 6.493557544708E+03
     2.196000000000E+05-1.797452569008E-07 5.461126718077E-01 1.234002411366E-07
     9.182063694952E-02-6.814062500000E+01 1.785066875978E+00-6.838141978918E-09
     6.975290548850E-10 0.000000000000E+00 7.880000000000E+02 0.000000000000E+00
     2.000000000000E+00 0.000000000000E+00 4.220000000000E-08 4.220000000000E-08
     2.196276000000E+05 1.000000000000E+00
C59 2021 02 09 14 00 00-9.402865543962E-07-3.552713678801E-14 0.000000000000E+00
     3.000000000000E+00 6.779531250000E+02 8.598215293037E-09-2.474760937166E+00
     2.227537333965E-05 2.083878498524E-04-8.258968591690E-06 6.493548173904E+03
     2.232000000000E+05-1.396983861923E-07 7.823465162841E-01 1.103617250919E-07
     9.700382299859E-02 2.483750000000E+02 1.562259061652E+00-7.583530170185E-09
     5.675236396376E-10 0.000000000000E+00 7.880000000000E+02 0.000000000000E+00
     2.000000000000E+00 1.000000000000E+00 4.220000000000E-08 4.220000000000E-08
     2.232276000000E+05 1.000000000000E+00
C59 2021 02 09 15 00 00-9.405193850398E-07-5.329070518201E-14 0.000000000000E+00
     4.000000000000E+00 5.583750000000E+02 9.137166313938E-09-2.233927387128E+00
     1.823995262384E-05 2.110612113029E-04-1.706136390567E-05 6.493535461426E+03
     2.268000000000E+05-7.683411240578E-08 1.008527392528E+00 9.173527359962E-08
     1.014806141835E-01 5.164375000000E+02 1.357628835399E+00-8.048549540109E-09
     4.103742365913E-10 0.000000000000E+00 7.880000000000E+02 0.000000000000E+00
     2.000000000000E+00 1.000000000000E+00 4.220000000000E-08 4.220000000000E-08
     2.268276000000E+05 1.000000000000E+00
```

Figure 1: Health marker for C59 in broadcast ephemeris on February 9, 2021.

in real time [7]. Huang et al. proposed an optimized robust detection method based on pseudorange observations, broadcast ephemeris, and known station coordinates [8]. Cui et al. used orbital residuals and mechanical models to detect orbital maneuvers of space targets; to accomplish this, they combined complex mechanical models [9]. Ye et al. used orbital differences before and after maneuvers to detect orbital maneuvers [10].

Nevertheless, these studies have only explored the detection models and methods of orbital maneuvering. They did not systematically analyze the performance of the proposed detection methods for multiple maneuvering events. This study combined BDS-3 with other global navigation satellite system (GNSS) to investigate 22 maneuvering events of two GEO satellites, C59 and C60, based on the analysis of the time-differenced carrier phase velocity measurement algorithm combined with data from different stations and broadcast ephemeris. Through detection and analysis, we determined the optimal threshold, system combination, and station location to identify the orbital maneuvers of the BDS-3 GEO satellites.

Section 2 of the study expounds on the maneuvering detection algorithm and experimental procedure. Section 3 details the data sources and results analysis, and Section 4 presents the conclusion and discussion.

2. Algorithms

The three-dimensional velocity of the station and the receiver clock offsets can be obtained using the time-differenced carrier phase velocity measurement in the event that no fewer than four satellites are observed by the station. Under normal circumstances, the measured station velocity must be zero or close to zero. However, when the satellites involved in the calculation conduct orbital maneuvers, their actual positions and ephemeris positions deviate substantially, such that a rapid adjustment process ensues, causing a substantial deviation in the calculated station velocity [10]. Based on this principle, an appropriate detection method can be established to detect the maneuvering period of satellites involved in the calculation.

This section first expounds on the principle of epoch differential velocity measurement, then introduces the method for determining BDS-3 satellite historical maneuvering and duration, and finally, demonstrates the design of the experimental procedure.

```
#dP2021  2  8  0  0  0.00000000     288   u+U IGb14 FIT  GFZ
## 2144  86400.00000000   300.00000000 59253 0.0000000000000
+  124   C01C02C03C04C05C06C07C08C09C10C11C12C13C14C16C19C20
+        C21C22C23C24C25C26C27C28C29C30C32C33C34C35C36C37C38
+        C39C40C41C42C43C44C45C46C59C60
```

(a)

```
#dP2021  2  9  0  0  0.00000000     288   u+U IGb14 FIT  GFZ
## 2144 172800.00000000   300.00000000 59254 0.0000000000000
+  123   C01C02C03C04C05C06C07C08C09C10C11C12C13C14C16C19C20
+        C21C22C23C24C25C26C27C28C29C30C32C33C34C35C36C37C38
+        C39C40C41C42C43C44C45C46C60
```

(b)

```
#dP2021  2 10  0  0  0.00000000     288   u+U IGb14 FIT  GFZ
## 2144 259200.00000000   300.00000000 59255 0.0000000000000
+  123   C01C03C04C05C06C07C08C09C10C11C12C13C14C16C19C20C21
+        C22C23C24C25C26C27C28C29C30C32C33C34C35C36C37C38C39
+        C40C41C42C43C44C45C46C59C60
```

(c)

Figure 2: Precision ephemeris of BDS satellites calculated by the GFZ on February 8 (a), 9 (b), and 10 (c), 2021.

2.1. Estimation of Velocity. The observation equation of the carrier phase can be expressed as [11, 12],

$$\lambda\Phi = d + c(\delta t_r - \delta t_s) + \lambda N + \delta d_{\text{eph}} - \delta d_{\text{ion}} + \delta d_{\text{trop}} + \varepsilon, \quad (1)$$

where λ is the wavelength, Φ is the carrier phase observation, d is the geometric distance between the station and satellite, c is the speed of light, δt_r is the receiver clock offsets, δt_s is the satellite clock offsets, N is the integer ambiguity, δd_{eph} is the ephemeris error, δd_{ion} is the ionospheric error, δd_{trop} is the slant tropospheric delay, and ε is the path and receiver noise. The cycle slip is detected by the combination of phase geometry-free combination, the Melbourne-Wübbena (MW) combination, and code-phase combination, with the thresholds all being empirical thresholds [13–16]. The difference between adjacent epochs was considered for the carrier phase observation (Equation (1)).

$$\lambda\Delta\Phi_{(t1,t2)} = \lambda[\Phi_{t2} - \Phi_{t1}] = \Delta d_{(t1,t2)} - c\Delta\delta t_{r(t1,t2)} + c\Delta\delta t_{s(t1,t2)} - \Delta d_{ion(t1,t2)} + \Delta d_{\text{trop}(t1,t2)} + \Delta\varepsilon_{(t1,t2)}, \quad (2)$$

where Δ is a single difference operator between the epochs. After a differential operation, the effect of integer ambiguity was eliminated, and the ionospheric and tropospheric delays were reduced. The ephemeris error between two consecutive epochs is usually almost the same constant, so δd_{eph} can be ignored. The satellite clock offsets can be corrected using ephemeris data. The first order of δd_{ion} was eliminated using a dual-frequency ionosphere-free model, and its high order is absorbed by residuals [17]. The Saastmoinen model and the global mapping function were used to obtain the tropospheric dry component delay and partial wet component delay, and the residual zenith tropospheric wet component delay was calculated by piecewise constant estimation [18–20].

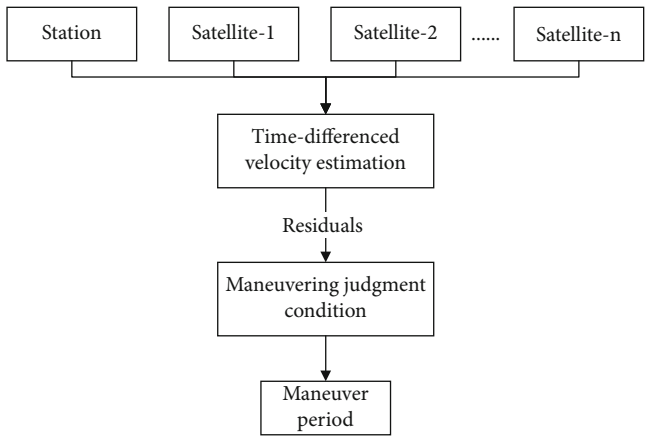

Figure 3: Flow chart of detection of maneuvering period.

The observation weights of the stochastic model can be set using Equation (3), where p is the observation weight and θ is the mean satellite elevation angle of two adjacent epochs [21, 22]. The least-squares method can be used to solve the three-dimensional velocity and

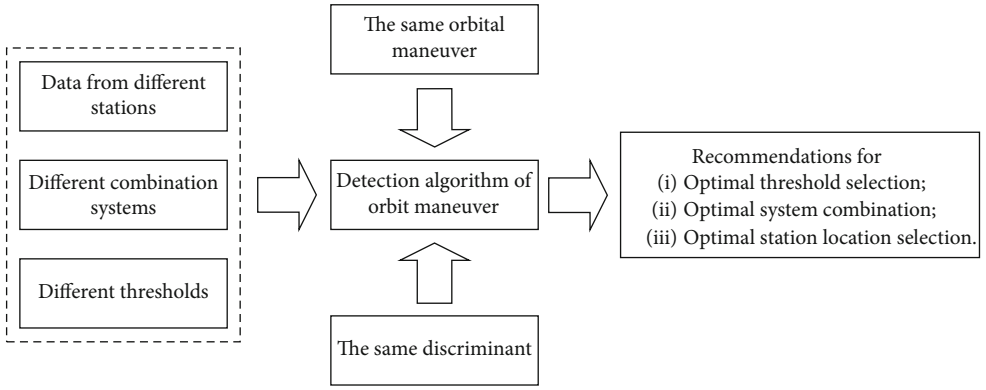

Figure 4: Implementation procedure for consistent and sensitive satellite orbit maneuver detection.

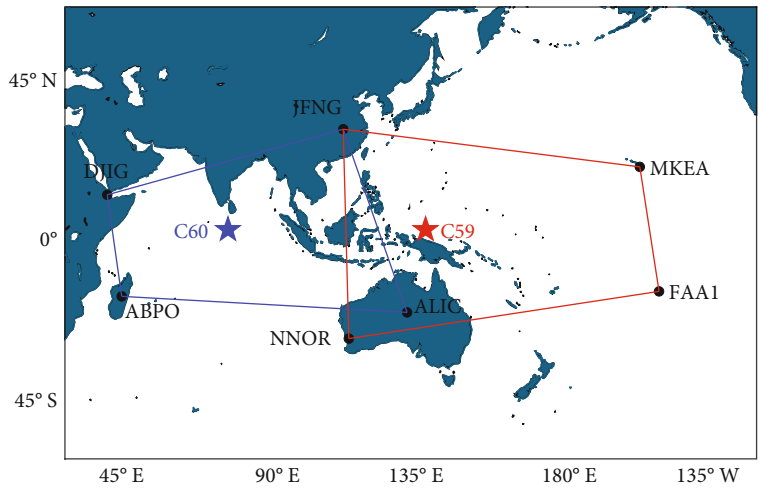

Figure 5: Locations of selected stations.

clock offsets of the receiver when there are at least four observation satellites.

$$p = \begin{cases} 1 & \theta \geq 30^{\circ}, \\ 2 \sin \theta & \theta < 30^{\circ}. \end{cases} \tag{3}$$

2.2. Identification of Maneuvering Satellites. This study is aimed at analyzing the consistency and sensitivity of the orbital maneuver detection of BDS-3 satellites because their orbital maneuvering information is not disclosed to the public. To perform an accurate statistical analysis of the historical maneuvers of BDS-3 satellites, this study determined the historical maneuvers of BDS-3 GEO satellites based on the BDS broadcast ephemeris health marker and the precise orbit products of the GeoForschungsZentrum Potsdam (GFZ).

Figure 1 shows the health marker of C59 for four consecutive hours in the broadcast ephemeris on February 9, 2021. Figures 2(a)–2(c) are the precise ephemeris of BDS satellites calculated by GFZ from February 8 to 10, 2021, respectively. At 14 : 00 on February 9, 2021, C59 was marked as unhealthy in the broadcast ephemeris. Meanwhile, the precise orbit products of C59 are not calculated by GFZ. Therefore, C59 can be considered to have undergone an orbital maneuver on that day [8].

Table 1: Details of the selected stations.

Station	Receiver	Antenna
DJIG	SEPT POLARX5	TRM59800.00
ABPO	SEPT POLARX5	ASH701945G_M
ALIC	SEPT POLARX5	LEIAR25.R3
JFNG	Trimble Alloy	TRM59800.00
NNOR	SEPT POLARX5TR	SEPCHOKE_B3E6
MKEA	SEPT POLARX5	JAVRINGANT_DM
FAA1	SEPT POLARX5	LEIAR25.R4

2.3. Detection of Maneuvering Period. Data verification demonstrated that the observation residuals were sensitive to orbital maneuvers. Therefore, the standard deviation (STD) of the observation residuals can be used to identify the start time of satellite maneuvers, and the observation residuals can be used to identify the end time of the satellite

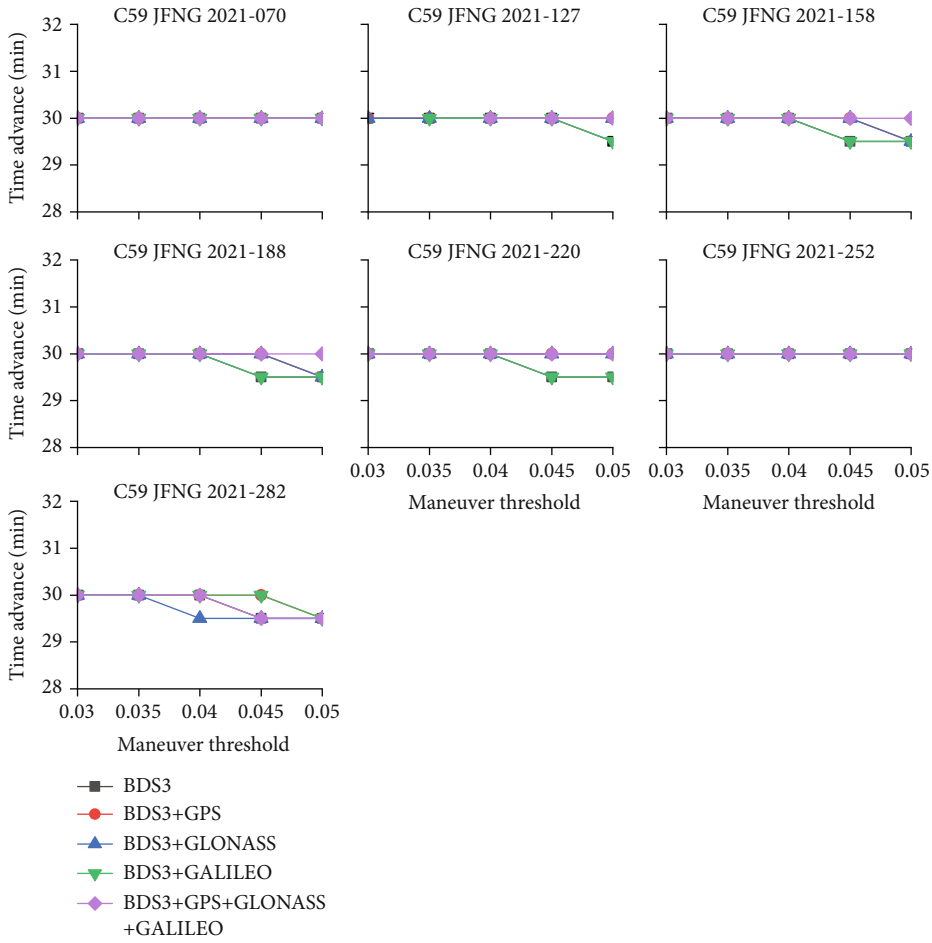

Figure 6: Comparison of detection results of C59 under different maneuvering thresholds.

maneuver. The start and end judgment conditions for a maneuver can be set as follows:

$$S(t) = \mathrm{STD}(t-29, t-28, \cdots, t) - S_m, (t \geq 29), \quad (4)$$

$$|0.1 \times R(t)| \geq |R(t+1), R(t+2), \cdots, R(t+10)|. \quad (5)$$

In Equation (4), $S(t)$ is the maneuver start judgment threshold at time t, $\mathrm{STD}(t-29, t-28, \cdots, t)$ is the standard deviation of the observation residuals of 30 epochs from time $t-29$ to time t, which can be calculated from Equation (6) and Equation (7). S_m is the maneuver threshold of satellite m, which is determined in subsequent chapters. Equation (5) is the judgment condition for the end of the maneuver, and $R(t)$ represents the observation residual at time t, the operator "| |" is used to get the absolute value.

$$\mathrm{STD}(t-29, t-28, \cdots, t) = \sqrt{\frac{\sum_{i=0}^{29}(x(t-i)-\mu)}{30}}, \quad (6)$$

$$\mu = \frac{\sum_{i=0}^{29} x(t-i)}{30}. \quad (7)$$

If $S(t), S(t+1), \cdots, S(t+9) \geq 0$, that is, the value $S \geq 0$ for 5 min, it is considered that the orbital maneuver starts at time t. If Equation (5) holds after detecting the start of the orbital maneuver, it can be determined that the orbital maneuver of the satellite ends at time t. Figure 3 shows the flow chart of the detection of the orbital maneuver period.

2.4. Experimental Procedure. First, different maneuvering thresholds were used to detect the same maneuvering event, the effect of different thresholds on detection sensitivity was determined, and the optimal thresholds for C59 and C60 were established. Next, the same station data and maneuvering events were analyzed using a combination of five systems: BDS-3, BDS-3+GPS, BDS-3+GLONASS, BDS-3+Galileo, and BDS-3+GPS+GLONASS+Galileo. The judgment results were then compared and analyzed under the same system combination for data from stations at different geographical locations to determine the consistency of the identified satellite maneuvering periods. Finally, the optimal scheme for station location selection and satellite system combination for GEO satellite orbit maneuvering detection of BDS-3 was defined. The implementation process is illustrated in Figure 4.

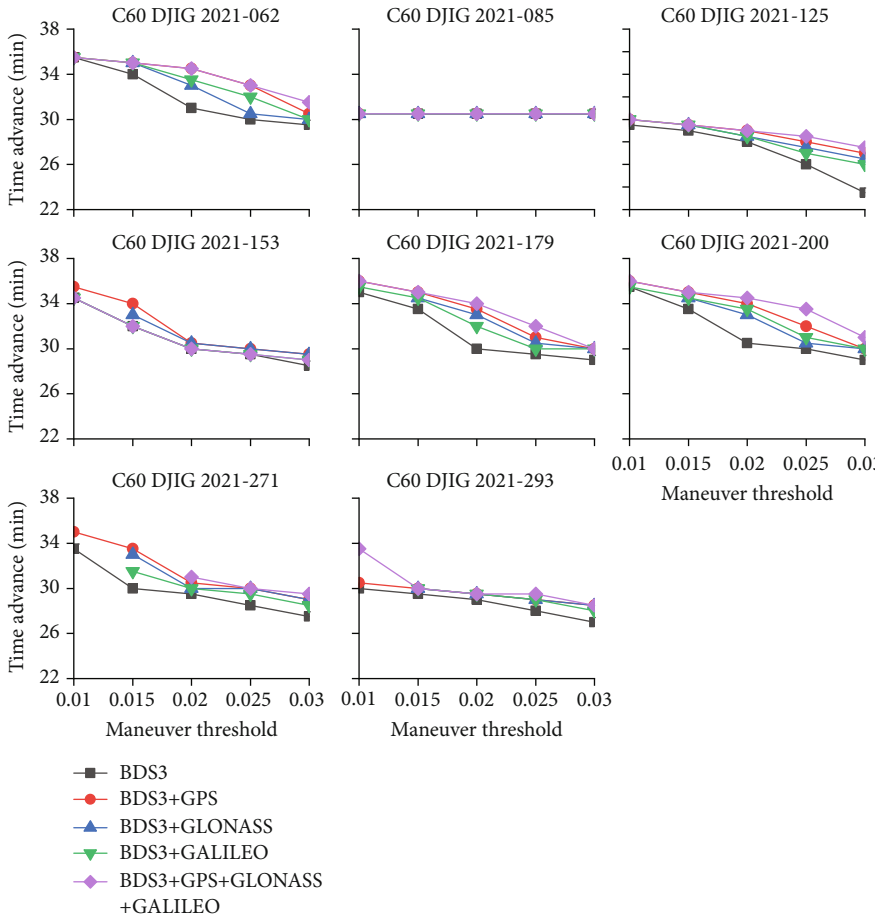

Figure 7: Comparison of detection results of C60 under different maneuvering thresholds.

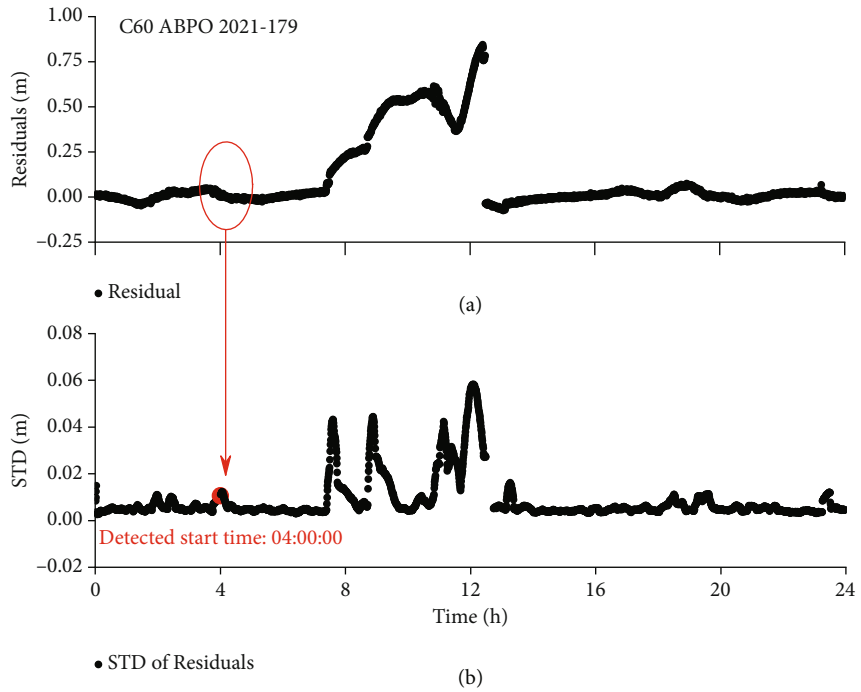

Figure 8: Time series of the residuals during the maneuver of the C60 satellite (a) and the maneuver decision diagram when the maneuver threshold is 0.01 (b).

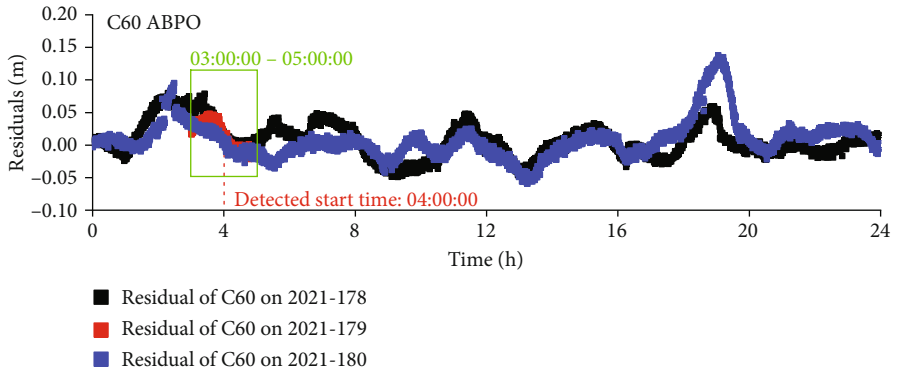

Figure 9: Comparison of the residuals one hour before and after the detected maneuver start time (green box) with the residuals when no maneuver occurred.

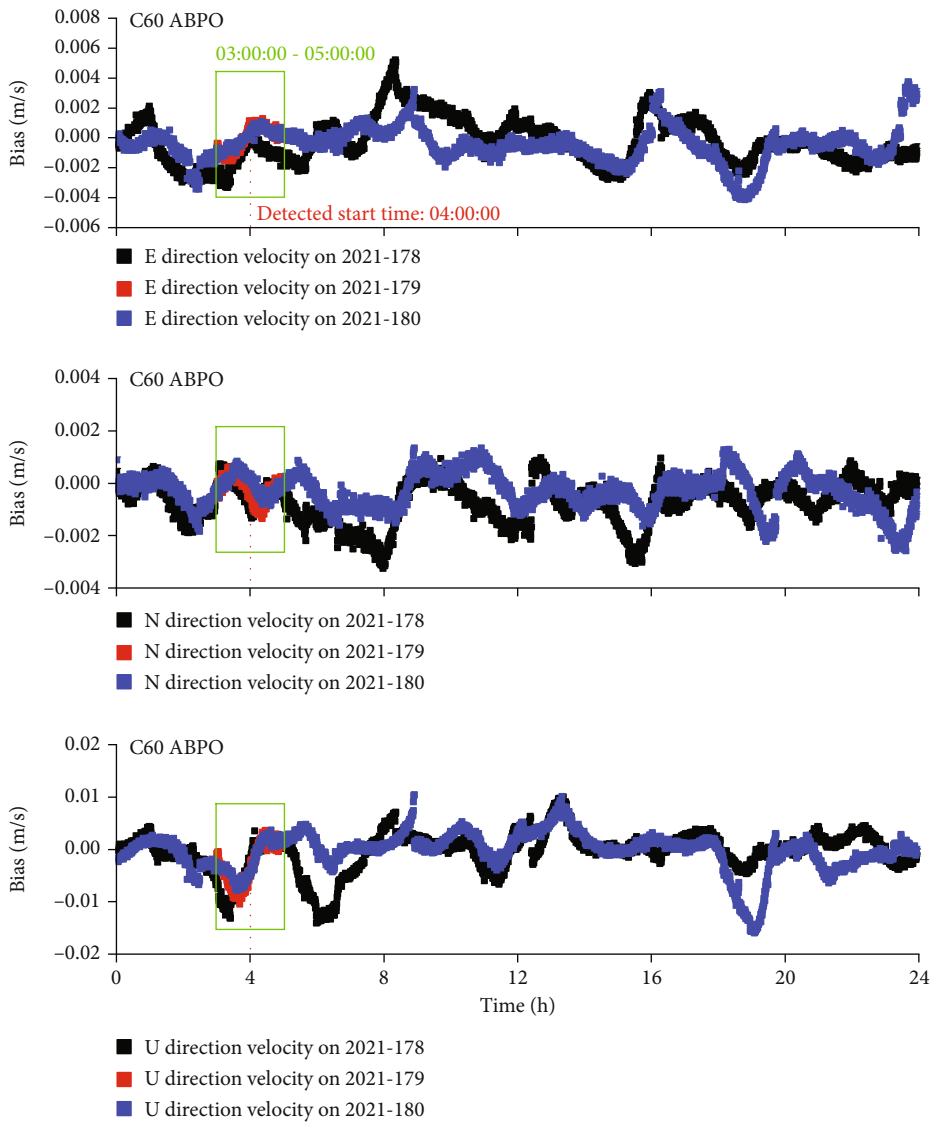

Figure 10: Comparison of the station velocity one hour before and after the detected maneuver start time (green box) with the station velocity when no maneuver occurred.

3. Verification and Results

Based on the surface projections of C59 and C60, seven stations were selected for analysis. Figure 5 illustrates the geographic distribution of the stations. The red and blue dots represent projections of C59 and C60 on the surface, respectively. The red line connects the stations selected by C59, and the blue line connects the stations selected by C60. The observation data sampling interval was 30 s, the broadcast ephemeris and satellite phase center correction data were obtained from the international GNSS service (IGS), and the earth rotation parameters (ERP) were provided by the center for orbit determination (CODE) in Switzerland. Table 1 summarizes the details of the selected stations.

3.1. Sensitivity. To determine the effects of different maneuvering thresholds on the detection sensitivity of the corresponding satellite orbital maneuvering start times, we empirically selected five maneuvering thresholds for C59 and C60. The detected maneuvering time and broadcast ephemeris marking time were compared and analyzed, and recommendations regarding optimal threshold selection were provided.

As different maneuvering thresholds do not affect the decision concerning the end time, this section only discusses the decision regarding the start time. Figures 6 and 7 depict the comparison between the detected maneuvering start times and broadcast ephemeris marking times under different thresholds. For the convenience of observation, the figures only illustrate the advancement of the maneuver start time detected by a single station for certain maneuvering events compared with the broadcast ephemeris. It can be observed that the advanced maneuvering start detected using different maneuvering thresholds of C59 is essentially the same and differs by only one epoch for individual maneuver events. For C60, with increasing maneuvering threshold, a significant downward trend was observed in the detected maneuvering start time.

Nevertheless, the detection sensitivity was higher when the maneuver threshold was smaller, which may cause the detection algorithm to misjudge the normal fluctuation of the residuals as an orbital maneuver. As shown in Figure 8, in the orbital maneuver of C60 on the 179th day in 2021, the maneuver start time detected by station ABPO was 04 : 00 : 00. Whereas, as shown in Figures 9 and 10, the residuals and the velocity of the station at this time are compared with the residuals and the velocity of the station when there is no maneuver in the adjacent two days, from the period 03 : 00 : 00–05 : 00 : 00, the residuals of C60 and the velocity of the station were within the normal range, indicating that no orbital maneuvering occurred during this period. Therefore, 0.045 and 0.02 were considered as the maneuvering thresholds for C59 and C60, respectively.

3.2. Consistency

3.2.1. Different GNSS Combinations. To verify the most suitable system combination for identifying GEO satellite orbit maneuvering during a specific satellite orbit maneuvering event, this study selected BDS-3, BDS-3+GPS, BDS-3+GLONASS, BDS-3+Galileo, and BDS-3+GPS+GLONASS+Galileo. Different combination systems were used to detect the maneuvering period, wherein each system was considered an equal-weight combination. Figure 11 illustrates the advancement of the maneuvering end time compared with the broadcast ephemeris marking time for C59 and C60 in dozens of maneuvering events detected by stations JFNG and DJIG. It was observed that the detected end times of orbital maneuvers were all approximately 30 min before the broadcast ephemeris marking time. For any maneuvering event, the detected maneuvering end times of the different system combinations are almost the same. Therefore, this section only presents a consistency analysis based on the maneuvering start times detected by different system combinations.

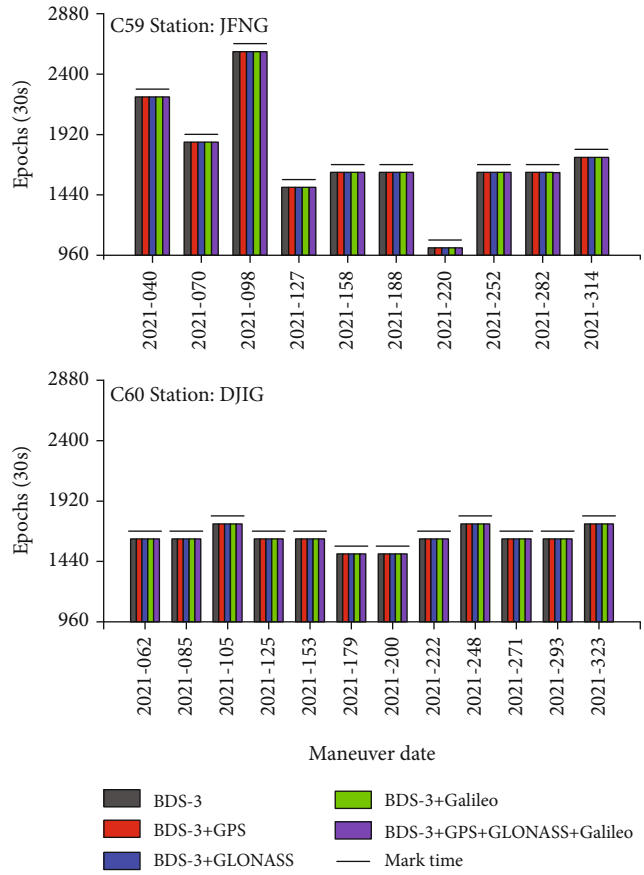

Figure 11: Comparison of detection results of C59 and C60 orbit maneuvering end time by different system combinations.

Figures 12 and 13 illustrate the comparison of the detection results for C59 and C60, respectively. Among them, the results of the 33rd detection of C59 and the 7th detection of C60 were not detected owing to missing data in the observation file. The negative value indicates that the detected maneuver time is later than the broadcast ephemeris marking time, which means that the detection sensitivity of this combination is relatively low.

Table 2 demonstrates mean advance of the C59 and C60 maneuver events detected by different system combinations.

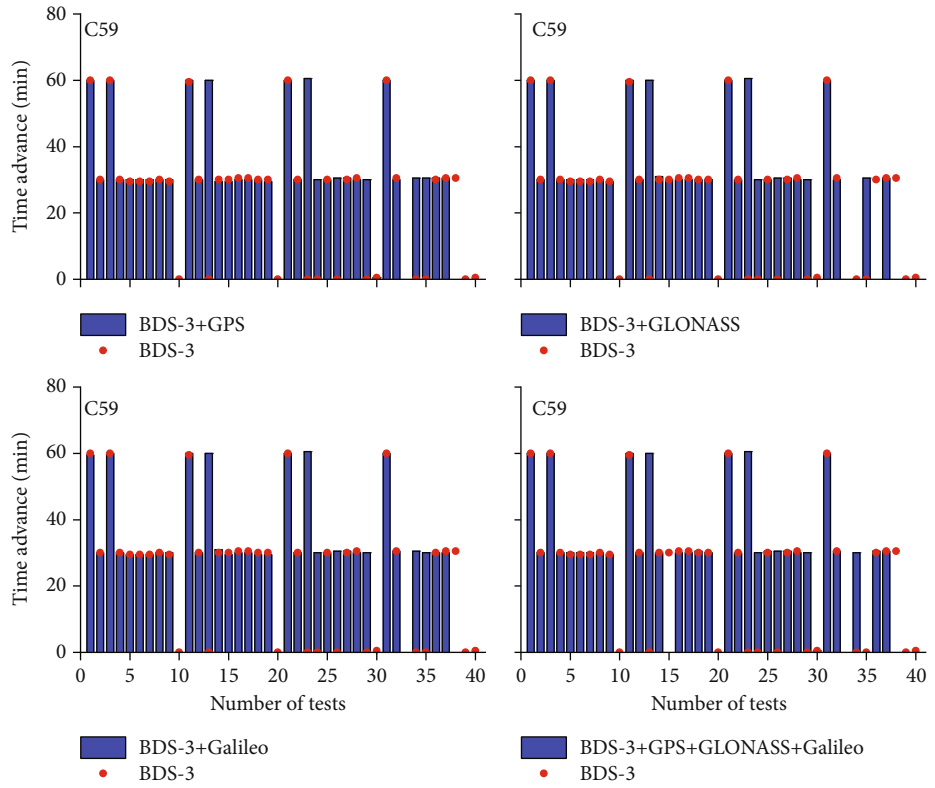

Figure 12: Comparison of detection results of C59 orbit maneuvering start times by different system combinations.

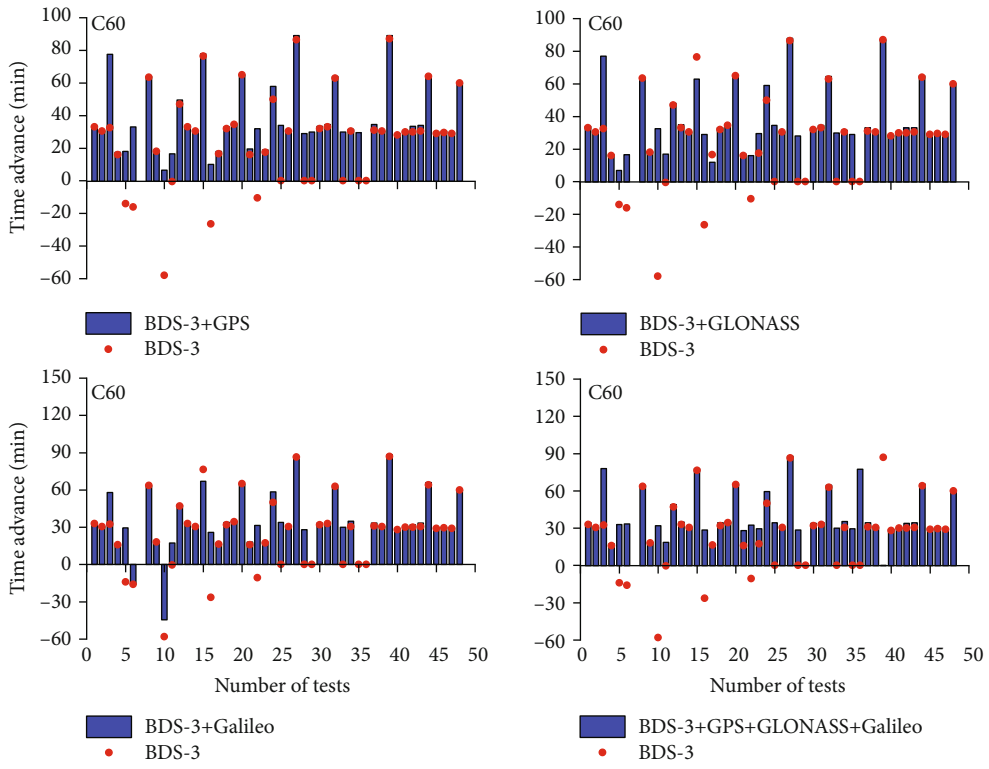

Figure 13: Comparison of detection results of C60 orbit maneuvering start times by different system combinations.

Table 2: Summary of C59 and C60 maneuvering start time detection by different combinations.

	Combination	BDS-3	BDS-3+GPS	BDS-3+GLONASS	BDS-3+Galileo	Four systems
C59	Mean advance (min)	33.92	34.03	34.07	33.98	34.10
C60	Mean advance (min)	28.84	37.15	36.74	34.25	39.46

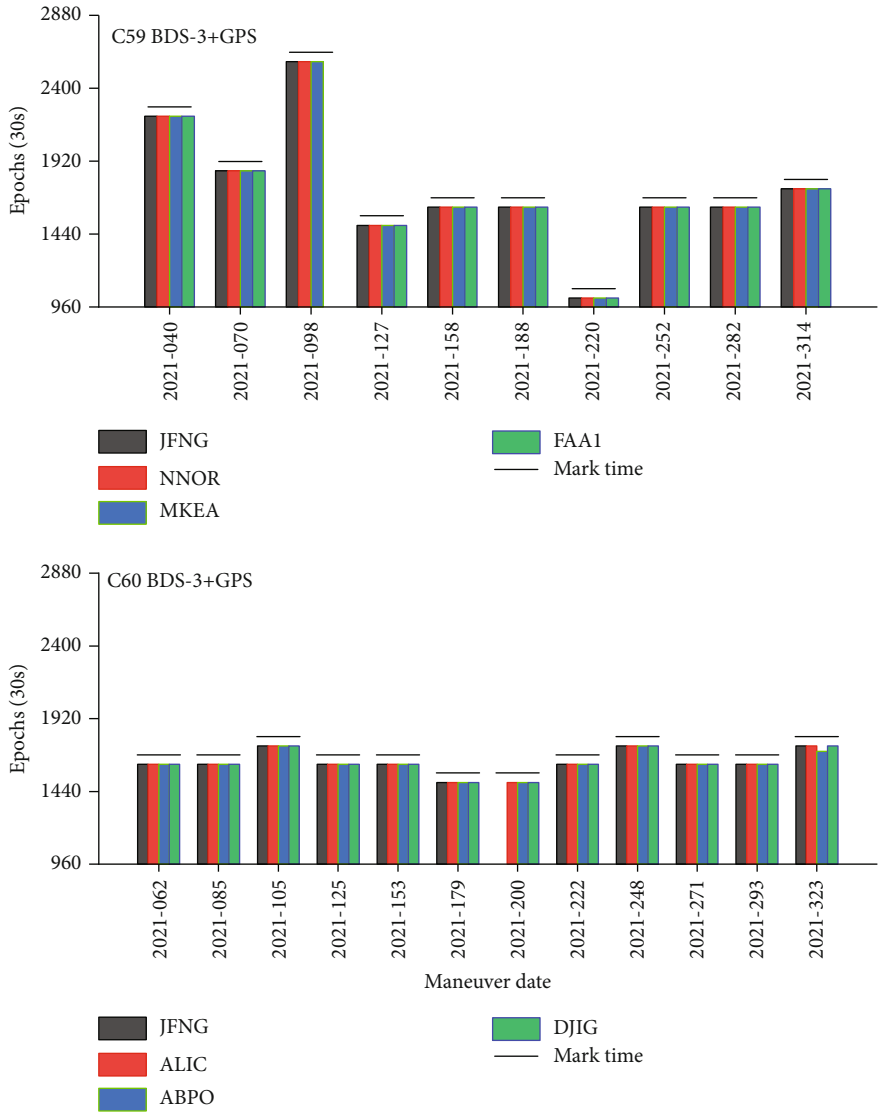

Figure 14: Comparison of detection results for C59 and C60 orbit maneuvering end times by different stations.

For C59, the orbit maneuvering start times detected by each combination were highly consistent with the mean advance of the broadcast ephemeris, with a difference of no more than 30 s. For the orbit maneuvering detection of C60, the selected combined systems (BDS-3+GPS, BDS-3+GLONASS, BDS-3+Galileo, BDS-3+GPS+GLONASS +Galileo) detected the maneuvering start time of C60 earlier than BDS-3 system 8.31, 7.90, 5.41, and 10.62 min, respectively.

Considering the computational complexity of the algorithm and the detected maneuvering periods, it can be concluded that the combination of BDS-3 and GPS can appropriately detect GEO maneuvering.

3.2.2. Different Stations. In Section 3.2, it was determined that the BDS-3+GPS combination was the most suitable for detecting the maneuvering of GEO satellites for BDS-3. Figure 14 shows a comparison of the detection results for the maneuvering end times of C59 and C60 detected at different stations using the combination of BDS-3+GPS, where the blank results were caused by missing data. It can be observed that the end times of the orbital maneuvers detected by different combinations were all approximately 30 min ahead of the broadcast ephemeris marking time. Additionally, for the same maneuver event, the end times of the orbital maneuvers detected by the different stations

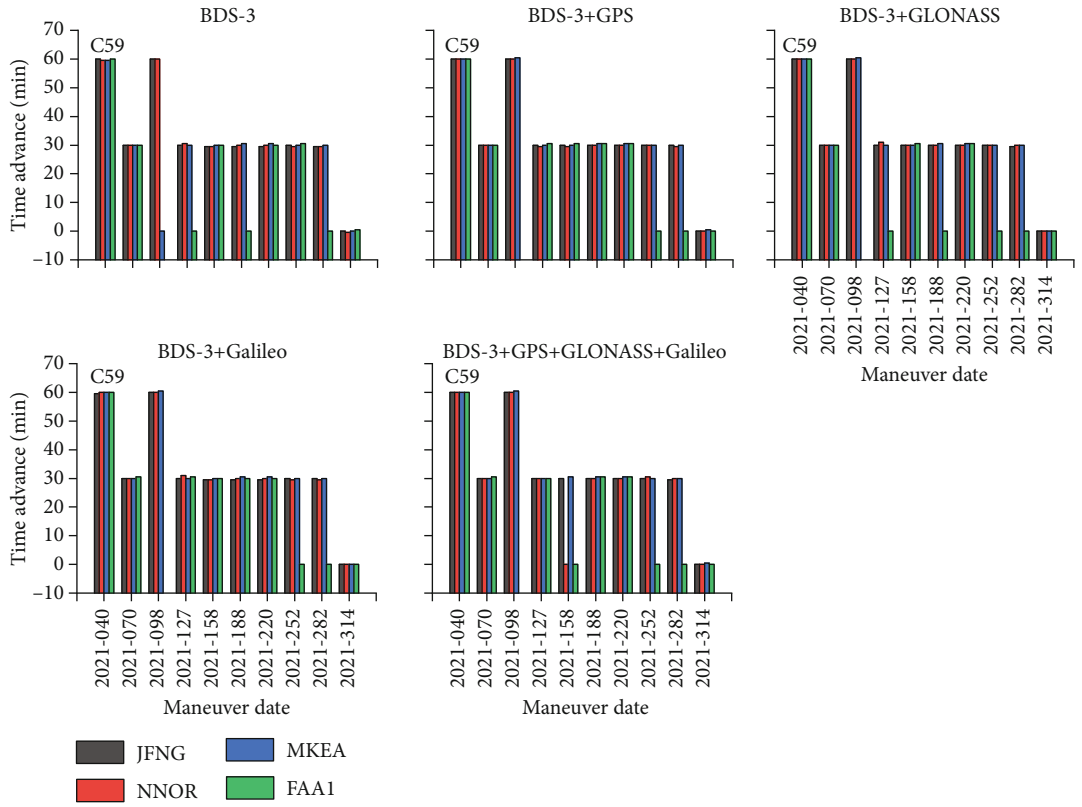

Figure 15: Comparison of detection results for C59 maneuvering start time by different stations using the same combined system.

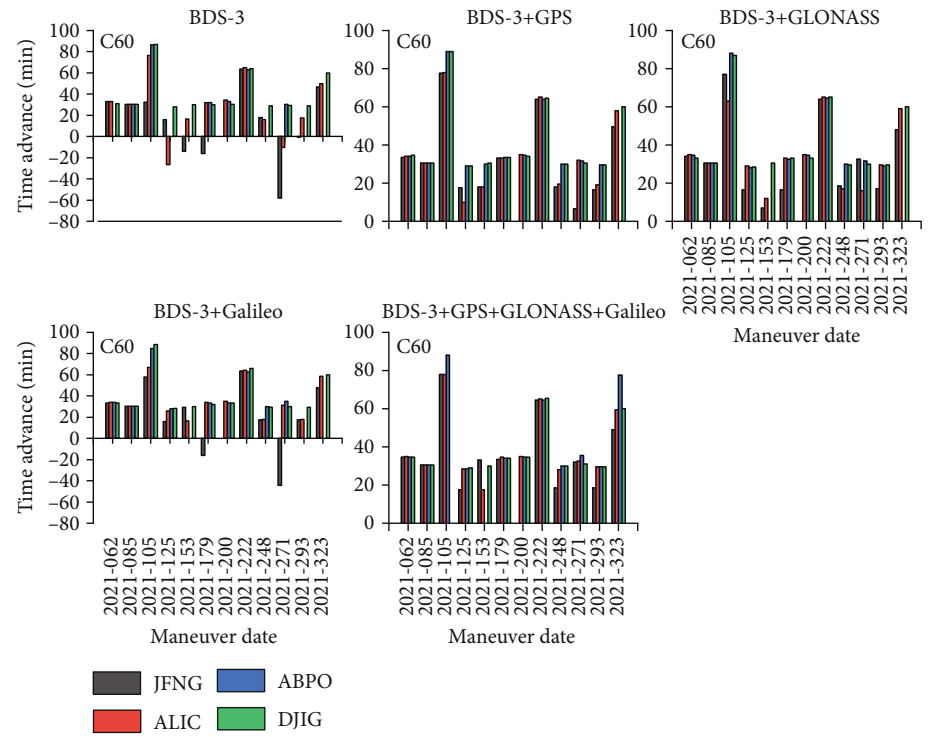

Figure 16: Comparison of detection results for C60 maneuvering start time by different stations using the same combined system.

Table 3: Summary of the start times of C59 and C60 maneuvers detected by different stations.

C59	Station	JFNG	NNOR	MKEA	FAA1
	Mean advance (min)	35.69	35.69	35.90	36
C60	Station	JFNG	ALIC	ABPO	DJIG
	Mean advance (min)	34.20	38.16	42.81	42. 42

were highly consistent. Therefore, only the detected orbital maneuver start times are analyzed in this section.

Figures 15 and 16 show a comparison of the detection results for the maneuvering start times of C59 and C60 satellites at different stations, respectively. The negative value indicates that the detected maneuver time is later than the broadcast ephemeris marking time, which means that the detection sensitivity of the station data to this maneuver is relatively low. Table 3 lists the average advance of the C59 and C60 maneuvering start times detected by each station compared to the broadcast ephemeris.

As shown in Figure 15, the start times of the same maneuvering event for the C59 satellite detected by different stations were essentially the same. Under the same system combination, the differences in the maneuvering start time measured by the four stations were less than 1 min, and the mean advance of the maneuvering start time was essentially the same, with a difference of no more than one epoch. Therefore, the effect of the station location on the orbital maneuver detection of the C59 satellite is negligible.

For C60, stations JFNG and ALIC located in Wuhan, China, and Alice Springs, Australia, respectively, detected the start time of the maneuver approximately 4.79–7.96 min later than stations ABPO and DJIG located in Antananarivo, Madagascar, and Observatoire Geophysique, Djibouti, respectively. As shown in Figure 16, during the maneuvering events of C60 that occurred on the 105th, 125th, 153rd, 248th, 293rd, and 323rd days in 2021, the maneuvering start times detected by ABPO and DJIG under the different system combinations were considerably earlier than those measured by JFNG and ALIC. By contrast, the maneuvering start times detected by the four stations for the other six maneuvering events were essentially the same. This situation may be related to the thrust direction and the observation geometry. In addition, because the maneuvering thrust of C60 is low, maneuvering detection is not noteworthy, and the response at the ground is weak.

4. Conclusion and Discussion

In this study, seven stations in different geographical locations were selected to detect 22 orbital maneuver events of the C59 and C60 satellites in 2021. To accomplish this, the BDS-3 system was combined with the GPS, GLONASS, and Galileo systems. The sensitivity and consistency of the orbit maneuver detection were determined, and the following conclusions were drawn:

(1) Small variations in the maneuvering threshold have a minor effect on the detection of orbital maneuvering of C59. However, the maneuvering threshold is extremely important for detecting the orbital maneuvering period of C60. The optimal maneuvering thresholds for C59 and C60 are 0.045 and 0.02, respectively

(2) Different system combinations were consistent in detecting the orbital maneuvers of C59. Additionally, the mean advance of the detected maneuver start time compared with the time marked by the broadcast ephemeris was less than 30 s. For C60, the combined system detected the start of maneuvers 8.31, 7.90, 5.41, and 10.62 min earlier than the BDS-3, respectively. Overall, the results point at BDS-3+GPS being the optimal system combination for orbital maneuver detection of C59 and C60

(3) Stations in different geographical locations were consistent in detecting orbital maneuvers of C59. The differences in the maneuvering start times detected by different stations were no more than 1 min, and the mean advance of the maneuver start time compared with the broadcast ephemeris was 35.69–36.00 min

(4) The maneuvers detected by the ABPO and DJIG stations in Africa were considerably earlier than those detected by the JFNG and ALIC stations in China and Australia, respectively, for half of all maneuvering events for C60; they were approximately 4.26–8.61 min earlier on average but were still adequately consistent

On this basis, we concluded that by selecting an appropriate threshold and combining BDS-3 with GPS, this method can perform orbital maneuvering detection of BDS-3 satellites within the visible range based on a single static station at different geographical locations. Future work should focus on real-time monitoring and repair of orbital maneuvers. If precise monitoring and repair of satellite orbit during maneuvers can be achieved, the recovery of the broadcast ephemeris data or precise orbit may be possible, which would greatly improve the quality of satellite services.

Data Availability

The data is available under request.

Conflicts of Interest

The authors declare that there is no conflict of interest regarding the publication of this paper.

Acknowledgments

This study was supported by the National Natural Science Foundation of China (grant nos.: 41974032 and 42274019).

References

[1] Y. X. Yang, L. Liu, J. L. Li et al., "Featured services and performance of BDS-3," *Science Bulletin*, vol. 66, no. 20, pp. 2135–2143, 2021.

[2] Y. X. Yang, W. G. Gao, S. R. Guo, Y. Mao, and Y. F. Yang, "Introduction to BeiDou-3 navigation satellite system," *Navigation*, vol. 66, no. 1, pp. 7–18, 2019.

[3] Y. L. Ge, X. Y. Cao, D. Lyu et al., "An investigation of PPP time transfer via BDS-3 PPP-B2b service," *GPS Solutions*, vol. 27, no. 2, 2023.

[4] R. Tu, R. Zhang, L. H. Fan et al., "Real-time monitoring of the dynamic variation of satellite orbital maneuvers based on BDS observations," *Measurement*, vol. 168, no. 1, article 108331, 2021.

[5] T. Creel, A. J. Dorsey, P. J. Mendicki, J. C. Little, R. G. Mach, and B. A. Renfro, "Summary of accuracy improvements from the GPS legacy accuracy improvement initiative (L-AII)," in *20th International Technical Meeting of the Satellite Division of the Institute of Navigation*, pp. 2481–2498, Fort Worth, TX, USA, 2007.

[6] L. Du, Z. K. Zhang, X. J. Li, R. P. Wang, L. Liu, and R. Guo, "Station-keeping maneuver monitoring and moving-window ground track fitting of GEO satellites," *Acta Geodetica et Cartographica Sinica*, vol. 43, no. 3, pp. 233–239, 2014.

[7] R. Tu, R. Zhang, P. Zhang, J. Han, L. Fan, and X. Lu, "Recover the abnormal positioning, velocity and timing services caused by BDS satellite orbital maneuvers," *Satellite Navigation*, vol. 2, no. 1, p. 16, 2021.

[8] G. W. Huang, Z. W. Qin, Q. Zhang, L. Wang, X. Y. Yan, and X. L. Wang, "An optimized method to detect BDS Satellites' orbit maneuvering and anomalies in real-time," *Sensors*, vol. 18, no. 3, p. 726, 2018.

[9] H. Z. Cui, W. L. Liu, G. S. Tang, B. Y. Song, and M. R. Ge, "Different thrust maneuvers detection of uncooperative space objects," *Journal of Astronautics*, vol. 37, no. 3, pp. 253–261, 2016.

[10] F. Ye, Y. Yuan, B. Tan, and J. Ou, "A robust method to detect BeiDou navigation satellite system orbit maneuvering/anomalies and its applications to precise orbit determination," *Sensors*, vol. 17, no. 5, p. 1129, 2017.

[11] W. D. Ding and J. L. Wang, "Precise velocity estimation with a stand-alone GPS receiver," *Journal of Navigation*, vol. 64, no. 2, pp. 311–325, 2011.

[12] P. Freda, A. Angrisano, S. Gaglione, and S. Troisi, "Time-differenced carrier phases technique for precise GNSS velocity estimation," *GPS Solutions*, vol. 19, no. 2, pp. 335–341, 2015.

[13] K. Wang and M. Rothacher, "Ambiguity resolution for triple-frequency geometry-free and ionosphere-free combination tested with real data," *Journal of Geodesy*, vol. 87, no. 6, pp. 539–553, 2013.

[14] Z. Dai, S. Knedlik, and O. Loffeld, "Real-time cycle-slip detection and determination for multiple frequency GNSS," in *2008 5th Workshop on Positioning, Navigation and Communication*, pp. 37–43, Hannover, Germany, 2008.

[15] C. S. Cai, Z. Z. Liu, P. F. Xia, and W. J. Dai, "Cycle slip detection and repair for undifferenced GPS observations under high ionospheric activity," *GPS Solutions*, vol. 17, no. 2, pp. 247–260, 2013.

[16] Z. Dai, K. Stefan, and L. Otmar, "Instantaneous triple-frequency GPS cycle-slip detection and repair," *International Journal of Navigation and Observation*, vol. 2009, Article ID 407231, 15 pages, 2009.

[17] A. Leick, L. Rapoport, and D. Tatarnikov, *GPS Satellite Surveying*, John Wiley & Sons, Inc, Hoboken, New Jersey, United States, 4th edition, 2015.

[18] J. Saastamoinen, "Atmospheric correction for the troposphere and the stratosphere in radio ranging satellites," *Geophysical Monograph Series*, vol. 15, pp. 247–251, 2013.

[19] J. Boehm, A. Niell, P. Tregoning, and H. Schuh, "Global mapping function (GMF): a new empirical mapping function based on numerical weather model data," *Geophysical Research Letters*, vol. 33, no. 7, 2006.

[20] J. Bohm, G. Moller, M. Schindelegger, G. Pain, and R. Weber, "Development of an improved empirical model for slant delays in the troposphere (GPT2w)," *GPS Solutions*, vol. 19, no. 3, pp. 433–441, 2015.

[21] P. L. Xu, C. Shi, R. X. Fang et al., "High-rate precise point positioning (PPP) to measure seismic wave motions: an experimental comparison of GPS PPP with inertial measurement units," *Journal of Geodesy*, vol. 87, no. 4, pp. 361–372, 2013.

[22] R. Tu, L. Wang, and Z. Liu, "Real time monitoring ground motion using GPS with real time corrections," *Survey Review*, vol. 48, no. 347, pp. 79–85, 2016.